Impact of parameter mismodeling on gravitational-wave searches

A Dissertation Submitted
in Partial Fulfilment of the Requirements
for the

MASTER OF SCIENCE

in

PHYSICS

by

Akshita Mittal
(Roll No. IMS19027)

to

SCHOOL OF PHYSICS
INDIAN INSTITUTE OF SCIENCE EDUCATION AND RESEARCH
THIRUVANANTHAPURAM - 695 551, INDIA

April 2024

DECLARATION

I, **Akshita Mittal (Roll No: IMS19027)**, hereby declare that, this report entitled **"Impact of parameter mismodeling on gravitational-wave searches"** submitted to Indian Institute of Science Education and Research Thiruvananthapuram towards the partial requirement of **Master of Science** in **Physics**, is an original work carried out by me under the supervision of **Dr. Soumen Basak** and has not formed the basis for the award of any degree or diploma, in this or any other institution or university. I have sincerely tried to uphold academic ethics and honesty. Whenever a piece of external information or statement or result is used then, that has been duly acknowledged and cited.

Thiruvananthapuram - 695 551 **Akshita Mittal**
April 2024

CERTIFICATE

This is to certify that the work contained in this project report entitled **"Impact of parameter mismodeling on gravitational-wave searches"** submitted by **Akshita Mittal** (**Roll No: IMS19027**) to Indian Institute of Science Education and Research, Thiruvananthapuram towards the partial requirement of **Master of Science** in **Physics** has been carried out by her under my supervision and that it has not been submitted elsewhere for the award of any degree.

Thiruvananthapuram - 695 551
April 2024

Dr. Soumen Basak
Project Supervisor

ACKNOWLEDGEMENT

I extend my sincere and profound gratitude to everyone who played a pivotal role in driving the project to this stage. I would like to express my heartfelt appreciation to my supervisors, Dr. Soumen Basak and Kallol Dey, for their invaluable guidance, feedback, and unwavering encouragement throughout the project. Their suggestions were immensely beneficial, and I am sincerely thankful for their constant support during the project. I especially thank Kallol for making time outside the schedule of this project and always answering my queries and questions. I also extend my gratitude to the School of Physics and the Center for High-Performance Computing, IISER Thiruvananthapuram, for the provision of resources to carry out the project.

I extend my heartfelt gratitude to my parents, Drs. Sonika Jindal and Manoj Mittal, for their unwavering emotional support and motivation throughout the duration of my BS-MS degree. Their encouragement and belief in me were invaluable in keeping me motivated and focused, especially on difficult days. In the same light, I extend thanks to my closest friends who have stayed with me through college, and I wish them the best in the future. I am indebted to 'rain everywhere' and all its members for their companionship.

Thiruvananthapuram - 695 551 **Akshita Mittal**

ABSTRACT

Bayesian analysis (or Bayesian inference) is the most commonly used method to extract information from gravitational-wave signals. Estimating parameters requires 'template' waveforms, which are modeled with extreme mathematical and computational prowess. These templates map the waveform shapes to physical parameters. We demonstrate that mismodeling these templates induces bias in the estimated parameters. The parameters under consideration in this study are **spin** and **eccentricity**. This work is carried out for stellar mass systems ($\mathcal{M}_c \approx 30M_\odot$), and is extendable to massive black hole binaries (MBHBs), which will be a primary target of the upcoming Laser Interferometer Space Antenna (LISA). With upcoming detectors, it is imperative to have *accurate* templates to extract information from these gravitational-wave signals. It is also important to understand the amount of mismodeling that does not induce a statistically significant bias in the posterior distributions of the estimated parameters. In this work, we show that even the slightest mismodeling induces statistically significant biases, especially for eccentricity mismodeling, and highlight the importance of accurate waveform modeling for current and upcoming detectors to avoid loss of information. We also introduce a `PyCBC` plugin `teobecc` in this study, that can accurately model spins (up to 0.9) and eccentricities (up to 0.3). Our work can be used to understand the impact of mismodeling or omitting parameters for bodies relevant across various frequency ranges. Eccentricity and spin are critical for such systems, and their mismodeling should produce substantial biases.

Keywords: *Gravitational waves, Bayesian inference, waveform modeling, eccentricity*

Contents

1 Introduction

The Laser Interferometer Gravitational-wave Observatory (LIGO) has been detecting gravitational wave (GW) signals from binary black hole (BBH) mergers since 2015 [1]. Advanced LIGO was joined by Advanced Virgo in 2017 [2], and KAGRA in 2020 [3]. In addition to these operational detectors, new detectors with higher sensitivities in different frequency ranges are being designed. This system of GW detectors will be joined by the next generation of ground-based detectors like the Einstein Telescope (ET) [4] and the Cosmic Explorer (CE) [5], along with space-based LISA [6] and TianQin [7], which will allow (i) detection of more GWs from various sources, and (ii) capture a longer portion of the signals.

These GWs carry valuable information about the originating binary system, including details like the mass of each component and their sky position. Techniques such as matched filtering [8] are employed to detect the signal, wherein observed data is compared with theoretical waveform models (or approximants), referred to as templates. Typically, the matched filter output is computed across a vast array of templates covering the parameter space of anticipated signals, called a template bank. However, extracting precise physical properties and understanding the underlying physics of the system necessitates Bayesian analysis [9]. Through Bayesian analysis, posterior probability density functions of the unknown signal parameters, which characterize a particular model/binary system, are evaluated. Template-based searches can also be utilized for conducting tests of general relativity (GR) [10], and searches of dark matter [11].

However, the power of a template-based search comes with inherent risks: when the prior holds significantly more information than the likelihood, it exerts a dominant influence on the posterior probability distribution. This can result in substantial systematic biases, especially if the model fails to accurately depict natural phenomena. Moreover, mismodeling parameters in the templates can lead to biases in the estimated parameters. Thus, accurately modeling GWs is crucial to extract information from the obtained signals.

1.1 About waveform approximants

Waveform templates (or approximants) serve as dynamic instruments for extracting and characterizing GW signals. By imposing strong constraints on signal morphologies, they enable the extraction of faint events hidden within instrumental noise. These templates facilitate the mapping of waveform shapes to physical parameters, thereby facilitating the generation of posterior probability distributions for these parameters. However, generating waveforms that account for all parameters describing a GW signal is computationally expensive, and methods to minimize computational cost without loss of accuracy are constantly being developed. Al-

though post-Newtonian (PN) expansion [12] gives a good approximation of the inspiral stage, it fails to describe the merger and ringdown accurately. The most accurate waveforms to describe a GW event are generated by numerical relativity (NR) [13–15], but they are immensely expensive to compute, which makes them impractical to use for data analysis. NR surrogate models [16–20] combine PN and NR waveforms to generate a computationally efficient as well as accurate waveform model to study a GW event. A semi-analytic family of waveforms is the Effective-One-Body (EOB) approximants, which map the general-relativistic two-body problem to a test particle moving in an external metric [21]. Ref. [22] provides detailed information about various waveform models. Fig. 1.1 shows the validity of different approximants across a radial separation and mass range.

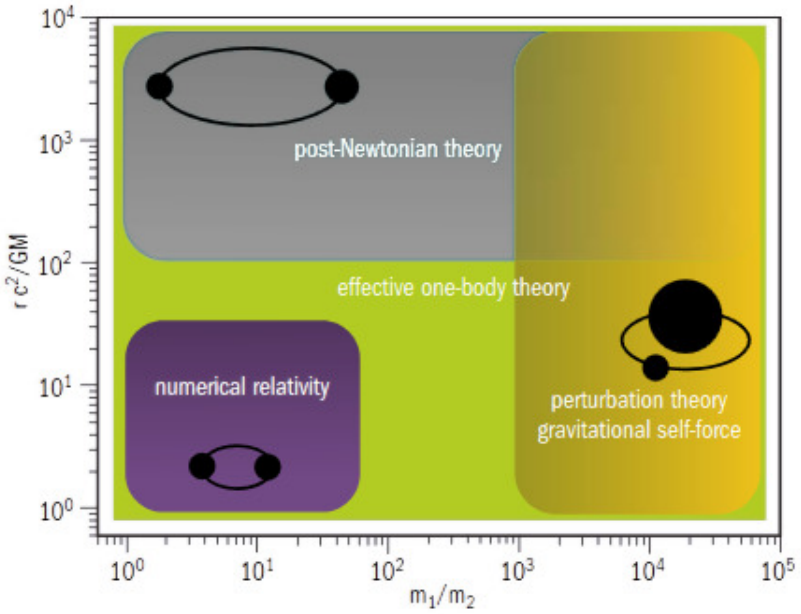

Figure 1.1: Current range of validity of the main analytical and numerical methods to solve the two-body problem. The horizontal axis shows the binary mass ratio, while the vertical axis shows the radial separation between the two black holes in the binary. Image and caption from [23].

1.1.1 Motivation

While no approximate waveform will be perfect, our focus lies in assessing whether these approximations suffice to analyze data collected by current and upcoming GW detectors. In this work, we try to understand the effect of mismodeling two parameters–**spin** and **eccentricity**, in terms of systematic biases induced in the parameter estimation of the source. For this, we consider the "worst" case of mismatch, with the parameter in consideration being set to 0. We will focus on stellar-mass systems with masses around 30-50 $M_\odot$. This study acts as a proof of concept due to limited computational resources and will be extended to masses of the order of $\mathcal{O}(10^6)M_\odot$, which are a potential target of the upcoming LISA mission.

1.2 About GW parameters

A GW signal is fully characterized by 15 parameters, assuming negligible orbital eccentricity. There are eight main properties, called "intrinsic" parameters, that define the binary system: the masses of the two black holes (called primary and secondary masses), and the spin vectors

for each. The other seven parameters are called "extrinsic" because they relate to how we observe the binary system: the angle of inclination, the angle of polarization, the phase when they merge, their position in the sky (right ascension and declination), the distance from us, and the time when they merge. In addition to these, information about sub-dominant modes and spin-induced precession helps to resolve degeneracies between parameters (illustrated in Fig. 1.3). Mismodeling these parameters can bias the posterior probability distributions of other parameters, thereby making the estimates unreliable. In this study, we try to understand the extent of bias induced by mismodeling spin and eccentricity.

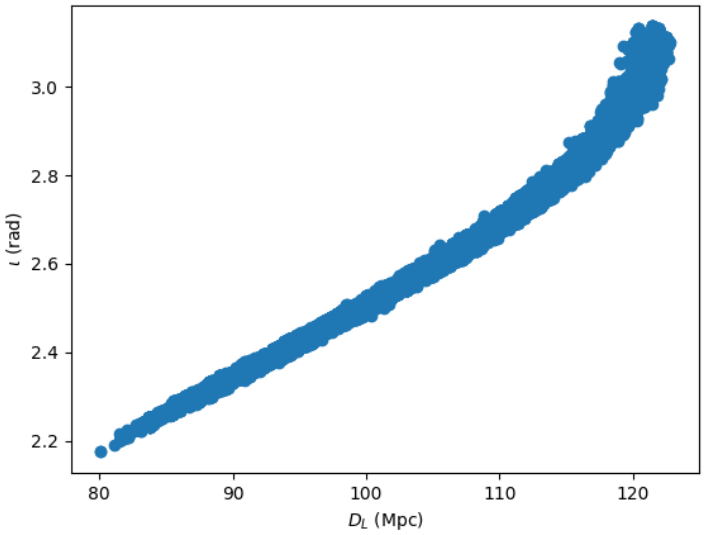

Figure 1.2: Scatter plot demonstrating degeneracy between luminosity distance and inclination. This degeneracy makes it difficult to place constraints on either of these parameters and estimate the sky location of the source. Inclusion of higher-order modes [24] and precession [25] helps resolve this degeneracy.

1.2.1 Why spin?

Spin is an important source parameter since details about the alignment of spins hold a multitude of information about the formation channel of the black hole. It is difficult to place constraints on individual values of spin because of the strong dependence of GW phase on effective spin ($\chi_{\rm eff}$) (defined in eq. 1.1). By measuring the effective spin distribution of the system, we can infer misalignment information, and, consequently, information about formation channels [26, 27]. The effects of mismodeling spin have been widely studied thus far. Introducing a mismatch between true and template spins can lead to incorrectly estimated parameters, particularly masses [28]. This is because of the correlation between mass ratio and spin components aligned with orbital angular momentum for individual bodies [29, 30]. In this study, we choose to analyze the impact of mismodeling spin as a benchmark to validate our approach.

$$\chi_{\rm eff} = \frac{(m_1\overrightarrow{\chi_1} + m_2\overrightarrow{\chi_2}) \cdot \hat{L}}{m_1 + m_2} \tag{1.1}$$

1.2.2 Why eccentricity?

Eccentricity is a smoking gun for the formation channels of binaries. Understanding the evolution of eccentricity of a binary in a globular cluster (GC) can hence clearly describe its dynam-

ical interactions with other bodies in the cluster [31]. Current extraction of GW signals all use circular orbital waveform templates, because the evolution of binary systems is generally considered to circularize due to GW radiation, i.e., they have negligible eccentricity when entering the LIGO detection band. A GW observation with a negligible eccentricity in the hecto-hertz band may have significant eccentricity in the space-based observation window. Furthermore, a wide range of eccentricity values in the LIGO band has been predicted by simulations of binary formations in GCs. Around 20% of BBHs formed through dynamical interactions are expected to have eccentricities exceeding 0.1 at 10 Hz [32], while approximately 1% of GC BBHs may exhibit eccentricities greater than 10^{-3} [33]. Other studies suggest that BBHs formed via 3-body interactions in globular clusters could represent up to 5% of the population, with eccentricities around 0.1 in the LIGO band [34]. It has been shown in [35] (and references therein) that even relatively small eccentricities ($e_0 \approx 10^{-3} - 10^{-2}$) can produce parameter biases.

The size of the parameter space makes it expensive to conduct parameter estimation for even signals that are a few seconds long. This motivates our work to understand the limit at which the bias induced by mismodeling a parameter becomes statistically significant to the posteriors of the estimated parameters.

1.3 About Bayesian inference

Bayesian analysis is a statistical method used to estimate parameters, θ, of a model, m, given some data, d. The method is based on the simple concept of Bayes' theorem,

$$P(A|B) = \frac{P(B|A)P(A)}{P(B)} \tag{1.2}$$

The conditional probability $P(B|A)$ refers to the *likelihood* and $P(A)$ refers to the *prior* probability of A. Bayes' theorem provides a relation to update a prior probability to the *posterior* probability $P(A|B)$ after observing B. In the context of data analysis, Bayes' theorem is

$$p(\boldsymbol{\theta}|\mathbf{d}, m) = \frac{L(\mathbf{d}|\boldsymbol{\theta}, m)\pi(\boldsymbol{\theta})}{Z} \tag{1.3}$$

The uncertainty of the parameters $\boldsymbol{\theta} = (\theta_1, .., \theta_p)$ before observing the data $\boldsymbol{d} = (d_1, ..., d_n)$ is expressed by the prior probability density function $\pi(\boldsymbol{\theta})$. $L(\mathbf{d}|\boldsymbol{\theta}, m)$ is the conditional probability density function of the data given unknown parameters and the model. The denominator Z is also called the *evidence* or the *marginal likelihood* and is merely a normalization constant. This normalization constant is not important for evaluating the posterior probability distributions.

To obtain the marginal posterior distribution of one parameter, it is necessary to integrate the joint posterior distribution over the remaining $p - 1$ parameters. Similarly, computing the posterior mean or variance entails additional integration [36]. Consequently, the primary challenge in Bayesian posterior computation arises when dealing with high-dimensional parameter spaces, as solving such integration problems becomes computationally demanding.

Analytical solutions are feasible only for conjugate priors, while numerical integration is viable solely in low dimensions. Gaussian approximations are applicable for unimodal and

symmetric posteriors, but simulation-based computational techniques are generally required. These techniques include Markov Chain Monte Carlo (MCMC) or nested sampling.

1.3.1 In GW data analysis

Let us look at what the components of Bayesian analysis constitute for GW data analysis.

The **data d** broadly represents the time series measurements of GW strain. For a network of K operational detectors, $\mathbf{d}^{(k)} = (d^{(k)}(t))$ is the strain measured at detector k. For sampling frequency f_s and captured signal length $\tau_{\rm obs}$ seconds, the time series in $\mathbf{d}$ consist of $T = f_s \times \tau_{\rm obs}$ measurements $d^{(k)}(t)$, with $t = 1, ..., T$. This data $d^{(k)}(t)$ is modeled as GW signal $h^{(k)}(t|\boldsymbol{\theta})$ buried in interferometer noise $n^{(k)}(t)$.

$$d^{(k)}(t) = h^{(k)}(t|\boldsymbol{\theta}) + n^{(k)}(t) \tag{1.4}$$

The noise $n^{(k)}(t)$ is generally assumed to be Gaussian and stationary. The strain depends on the parameters of the source (introduced in 1.2) and on the orientation of the detector with respect to the source. For polarizations h_+ and $h_\times$, this relative positioning of the detector is coded in antenna responses,

$$h^{(k)}(t|\boldsymbol{\theta}) = F_+^{(k)} h_+(t|\boldsymbol{\theta}) + F_\times^{(k)} h_\times(t|\boldsymbol{\theta}) \tag{1.5}$$

The exact nature of the $h_{+,\times}(t|\boldsymbol{\theta})$ depends on the emitting source and holds information about the source. In GW analysis, the parameter vector $\boldsymbol{\theta}$ consists of 15 parameters on which the **prior** $\pi(\boldsymbol{\theta})$ is placed. The Whittle likelihood [37] (eq. 1.6) is the most commonly used **likelihood** L in GW physics. The likelihood is assumed for each detector k, and the total likelihood is

$$L(\mathbf{d}|\boldsymbol{\theta}) = \prod_{i=1}^{K} L(\mathbf{d}^{(k)}|\boldsymbol{\theta}) \tag{1.6}$$

With all the components in place, we require sampling techniques to calculate the posterior probability distributions $p(\boldsymbol{\theta}|\mathbf{d})$. Although a multitude of sampling techniques have been developed, we employ implementations of two techniques – MCMC [38] and nested sampling [39] in this work.

Markov Chain Monte Carlo

MCMC, first introduced in [40], is a set of algorithms where points undergo a random walk through the posterior distribution. In this, the transition property of the Markov chain decides the probability of moving to any given point. We effectively generate samples from the posterior probability distribution by tracking the positions of these particles, often referred to as 'walkers,' at each iteration. An MCMC algorithm requires a "burn-in" phase, to ensure the walkers have settled into a steady state before collecting samples. Moreover, the positions of the walkers in the algorithm are auto-correlated, which necessitates "thinning" the chain. This selects samples separated by the auto-correlation length of the chain.

Nested Sampling

The differentiating aspect between MCMC and nested sampling is that nested sampling is primarily designed to calculate the evidence, and drawing samples from the posterior distribution is a by-product of the algorithm. Nested sampling populates the parameter space with "live points" drawn from the prior distribution. At each iteration, the lowest likelihood point is culled from the live set. New samples are drawn from the prior distribution until a point with a higher likelihood than the removed one is encountered. As the nested sampling algorithm progressively explores higher likelihood regions, it can estimate an upper bound on the evidence at each iteration. This information determines the termination criterion for this algorithm, causing it to stop once the current estimate of the evidence surpasses a certain fraction of the estimated upper limit.

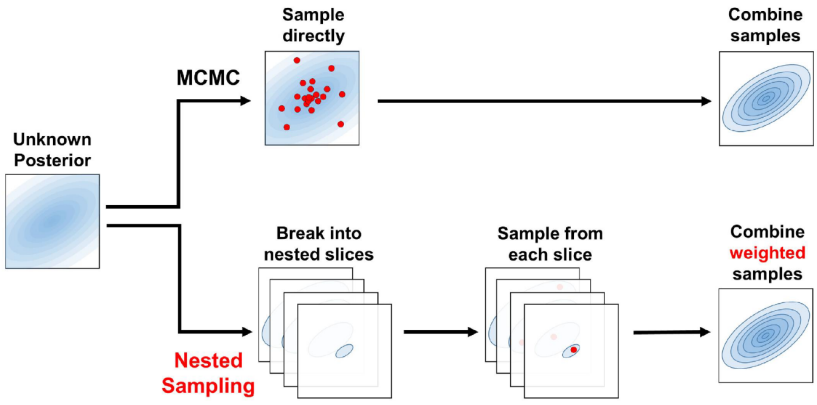

Figure 1.3: Demonstrative workflow of MCMC and nested sampling methods. Image from [41].

For this study, Bayesian analysis is comprehensively carried out using `PyCBC` [42].

2 Methods

In this section, we outline the workflow of the `pycbc_inference` module for the two parameters under consideration. It should be noted that this study uses stellar-mass binaries as sources, and acts as proof of concept of the effect of parameter mismodeling to be extended to MBHBs.

2.1 Analysis with `pycbc_inference`

Each case is termed a *test run*. The `pycbc_inference` module is a user-friendly approach to conduct parameter estimation of compact binary coalescences. We need to set up injection, prior, data and sampler configuration files for `pycbc_inference`.

2.1.1 Signal Injection

A signal injection is generated using `pycbc_create_injections`. For the scope of this work, we only generate one injection for each test run. For the spin analysis, `IMRPhenomD` [43] is used, and `teobecc` [44] is used for the eccentricity analysis. The parameters used for this study are listed in Tables 2.1 and 2.2.

2.1.2 Configuring the template

The templates are generated using the `IMRPhenomD` waveform for spin mismodeling analysis and the `teobecc` waveform to study eccentricity mismodeling. For the scope of this work, polarization, phase at coalescence, right ascension and declination are kept constant. For the spin mismodeling, masses, inclination, and distance are varied when the spin in the template is set to 0, and masses, inclination, distance, and spins are varied when eccentricity is set to 0 in the eccentricity mismodeling analysis.

2.1.3 Configuring the data

We generate fake strain colored by the Advanced LIGO updated design sensitivity curve throughout this analysis. The duration of the data to be analyzed is set in this file using the `analysis-(start|end)-time` arguments. This data should be long enough to contain the longest waveform taken by the prior as well as the timing uncertainty. Waveform duration, which is determined by the total mass of the system, is set to ≈ 6 seconds. We only choose 2 seconds after the trigger time to account for ringdown after the merger and uncertainty. The injection we provide is added to this data.

Data configuration also includes configuring the noise PSD, which is done using a Welch-like method. We use 512s of data centered at the trigger time for this estimation. We choose the segment length to be 8s, and the stride to be 4s. The data in each segment is transformed

to the frequency domain and two median values in each frequency bin from all segments are calculated and then averaged to obtain the PSD. We account for the corruption of the data caused by the convolution of inverse PSD with the data by subtracting 4s from the beginning and end of the data segment.

2.1.4 Configuring the sampler

This study uses only two samplers – `emcee_pt` [45, 46] and `dynesty` [47]. For the spin analysis, both `emcee_pt` and `dynesty` provide equivalent results, but the time of computation for `emcee_pt` is around 20 times higher than that of `dynesty`. For the spin analysis, we use `dynesty` with 2000 live points. Fig. 2.1 shows the similarity between estimates for the `dynesty` and `emcee_pt` samplers.

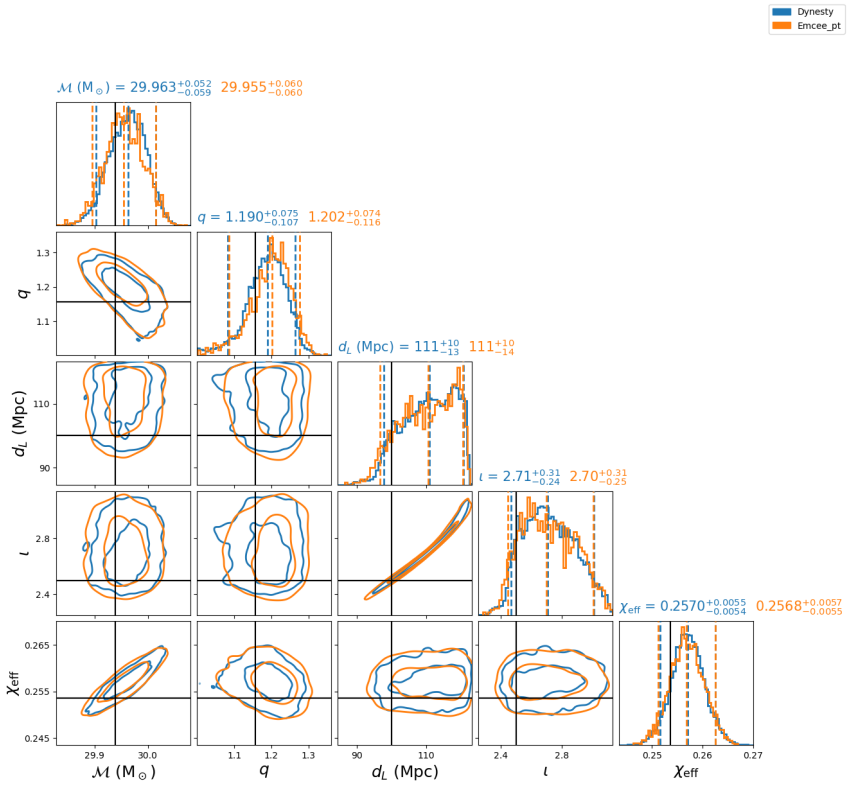

Figure 2.1: Comparison between the `dynesty` and `emcee_pt` samplers for spins 0.3 and 0.2. Black lines represent the injected parameter values of the signal. The tiles at the top of each column display the median and 90% range for each inference. The contour in the 2D tiles represents the 1-sigma and 2-sigma confidence intervals. Blue plots use `dynesty` and orange plots use `emcee_pt`.

On the contrary, we observe that `dynesty` fails to sample eccentricity properly, so we use the computationally expensive alternative for the eccentricity mismodeling analysis. The results presented here are produced with 1000 effective samples, 20 temperatures, and 50 walkers.

Throughout the analysis, sampling is done in terms of chirp mass and mass ratio instead of primary and secondary masses.

2.2 Adapting `pycbc_inference` for eccentric signals

To study the impact of eccentricity on parameter estimation, we require a waveform model with both spin and eccentricity. To achieve this, we utilize `PyCBC`'s waveform plugin feature and the

eccentric branch of the `TEOBResumS` waveform [48] to develop a plugin for our analysis. This waveform plugin, called `teobecc` can be locally installed and added to `PyCBC`, and ensures user-friendly implementation of the `pycbc_inference` module for eccentric and spinning systems.

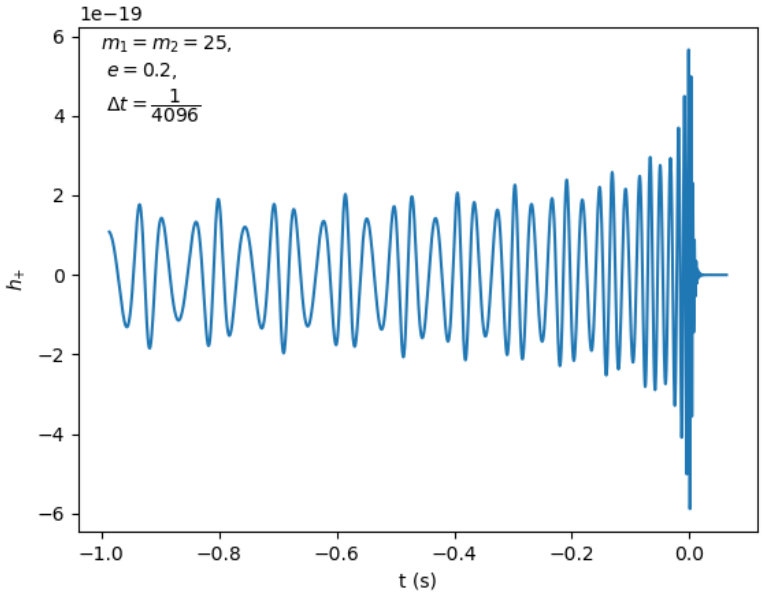

Figure 2.2: Time-domain plot of a stellar-mass signal with eccentricity 0.2 generated with `teobecc`. The presence of the signature of eccentricity confirms the correct implementation of `teobecc`.

2.3 Parameters for analysis

2.3.1 Spin Mismodeling

For the spin analysis, we consider $(\chi_{1z}, \chi_{2z}) = (0.5, 0.2)$, $(0.3, 0.2)$, $(0.3, 0.1)$, $(0.1, 0.1)$ and $(0, 0)$ along with the injection parameters in Table 2.1.

Parameter	Value
Chirp mass, $\mathcal{M}_c$ $(M_\odot)$	29.24
Mass ratio, q	1.15
Luminosity distance, D_L (Mpc)	100
Inclination, ι (rad)	2.5
Polarization, ψ (rad)	1.75
Coalescence phase, ϕ_c (rad)	1.5
Longitude, λ (rad)	2.2
Latitude, β (rad)	-1.25

Table 2.1: Source parameters for signal generation for a spinning stellar-mass system.

2.3.2 Eccentricity Mismodeling

For the eccentricity analysis, we consider e=0, 0.1, 0.2 along with the injection parameters in Table 2.2.

Parameter	Value
Chirp mass, $\mathcal{M}_c$ ($M_\odot$)	31.85
Mass ratio, q	1.31
Spin of primary along orbital angular momentum, χ_1	0.5
Spin of secondary along orbital angular momentum, χ_2	0.6
Luminosity distance, D_L (Mpc)	100
Inclination, ι (rad)	2.5
Polarization, ψ (rad)	1.75
Coalescence phase, ϕ_c (rad)	1.5
Longitude, λ (rad)	2.2
Latitude, β (rad)	-1.25

Table 2.2: Source parameters for signal generation for an eccentric stellar-mass system.

3 Results

In this section, we present the results of our spin and eccentricity analysis. The associated data release which contains all of the code and instructions on how to reproduce the results will be updated on [44] shortly. Documentation to use `pycbc_inference` can be found in [49].

3.1 Preliminary Analysis: Spin Mismodeling

To understand how spin mismodeling affects parameter estimation, we conduct Bayesian analysis for five spin cases with $(\chi_{1z}, \chi_{2z}) = (0.5, 0.2)$, $(0.3, 0.2)$, $(0.3, 0.1)$, $(0.1, 0.1)$ and $(0, 0)$. The posterior corner plots for all five cases are presented here.

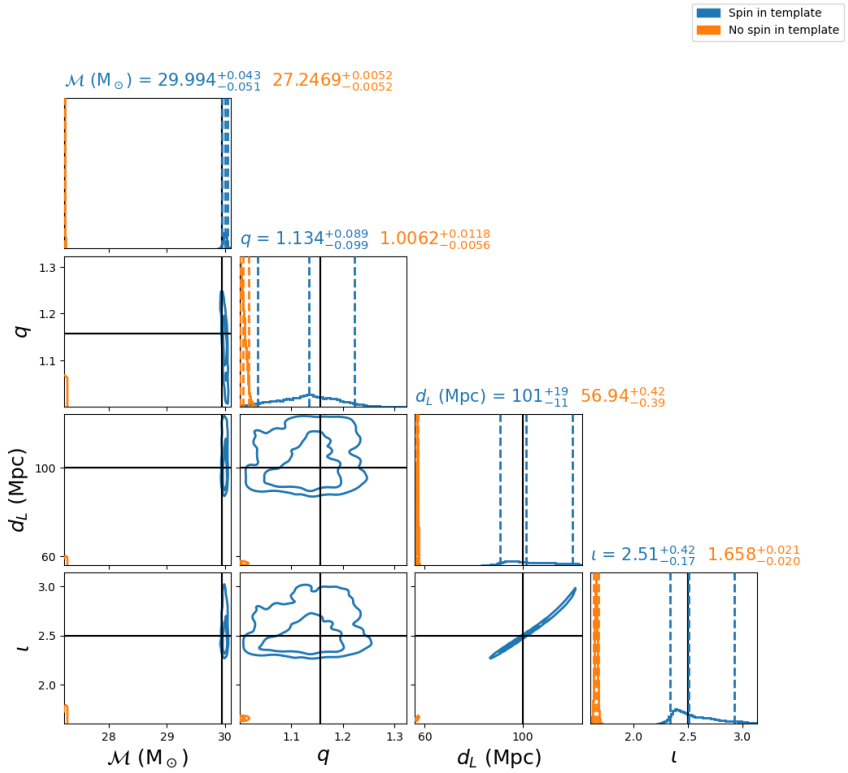

Figure 3.1: Parameter posterior corner plot of injected stellar-mass signal with spins 0.5 and 0.2 in Gaussian stationary noise. Black lines represent the injected parameter values of the signal. The tiles at the top of each column display the median and 90% range for each inference. The contour in the 2D tiles represents the 1-sigma and 2-sigma confidence intervals. Blue plots represent the case where spin is a variable parameter in the analysis and orange plots represent the case when spin is put to 0 in the template.

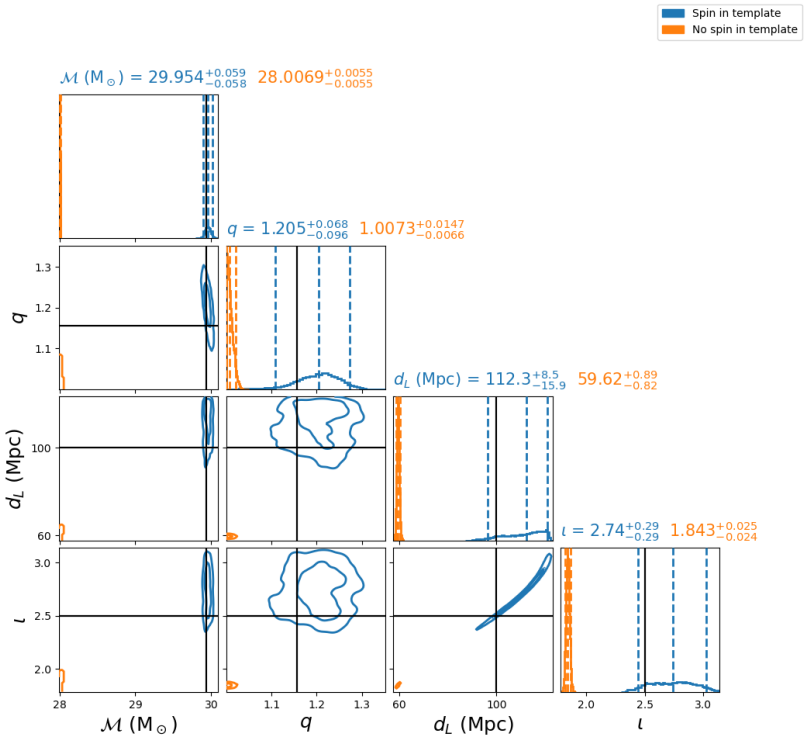

Figure 3.2: Parameter posterior corner plot of injected stellar-mass signal with spins 0.3 and 0.2 in Gaussian stationary noise. Black lines represent the injected parameter values of the signal. The tiles at the top of each column display the median and 90% range for each inference. The contour in the 2D tiles represents the 1-sigma and 2-sigma confidence intervals. Blue plots represent the case where spin is a variable parameter in the analysis and orange plots represent the case when spin is put to 0 in the template.

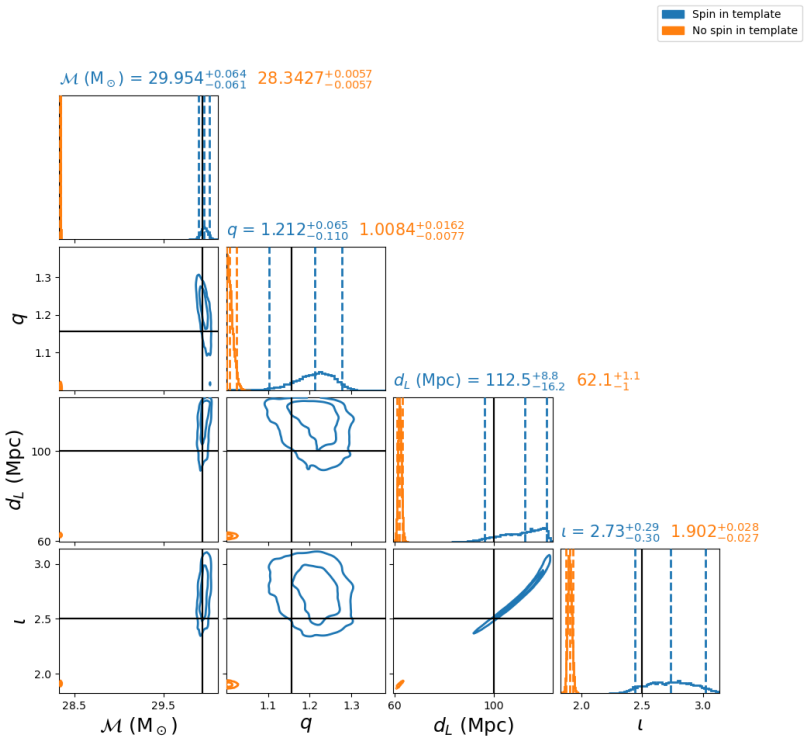

Figure 3.3: Parameter posterior corner plot of injected stellar-mass signal with spins 0.3 and 0.1 in Gaussian stationary noise. Black lines represent the injected parameter values of the signal. The tiles at the top of each column display the median and 90% range for each inference. The contour in the 2D tiles represents the 1-sigma and 2-sigma confidence intervals. Blue plots represent the case where spin is a variable parameter in the analysis and orange plots represent the case when spin is put to 0 in the template.

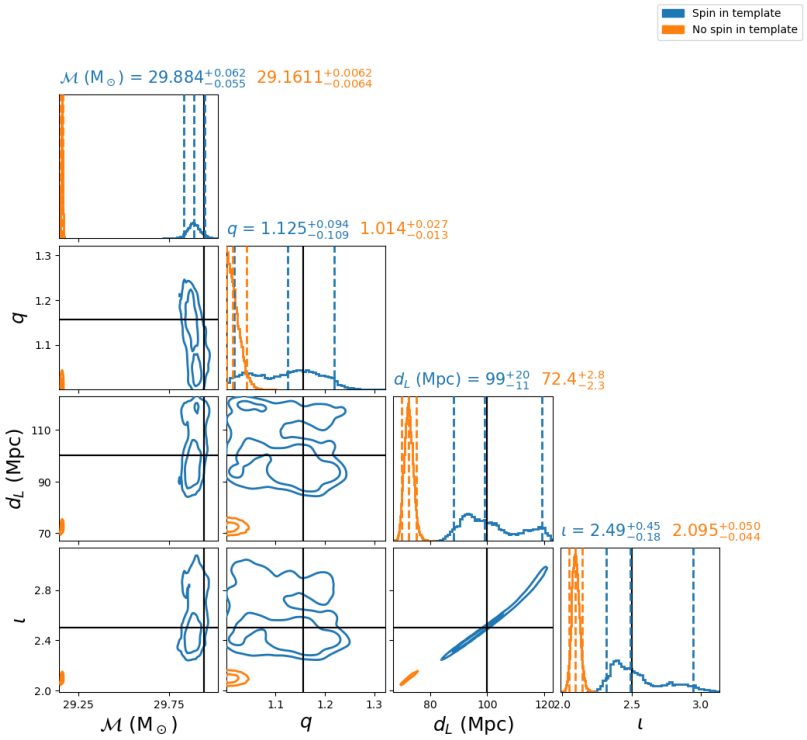

Figure 3.4: Parameter posterior corner plot of injected stellar-mass signal with spins 0.1 and 0.1 in Gaussian stationary noise. Black lines represent the injected parameter values of the signal. The tiles at the top of each column display the median and 90% range for each inference. The contour in the 2D tiles represents the 1-sigma and 2-sigma confidence intervals. Blue plots represent the case where spin is a variable parameter in the analysis and orange plots represent the case when spin is put to 0 in the template.

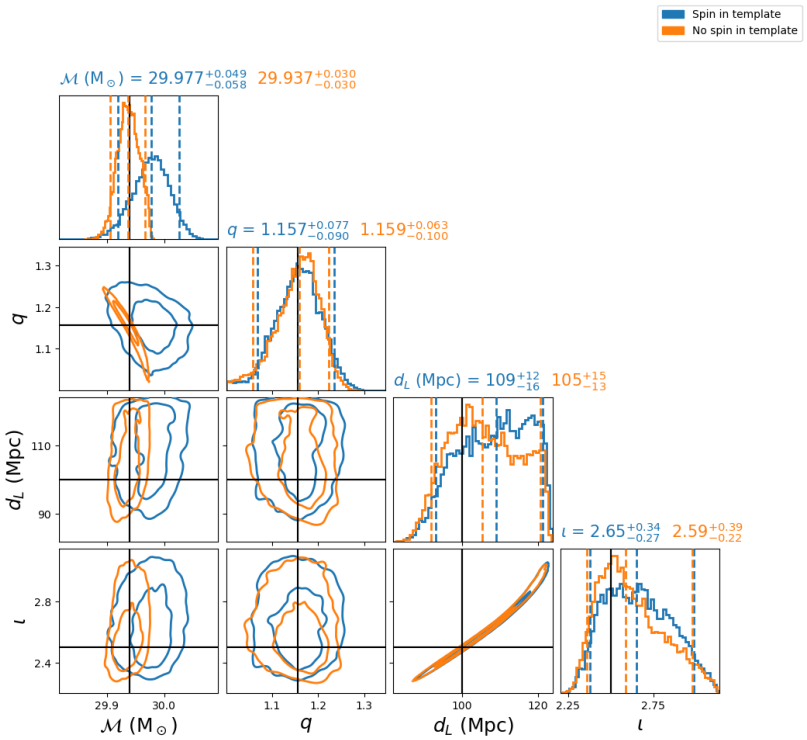

Figure 3.5: Parameter posterior corner plot of injected stellar-mass signal with spins 0 and 0 in Gaussian stationary noise. Black lines represent the injected parameter values of the signal. The tiles at the top of each column display the median and 90% range for each inference. The contour in the 2D tiles represents the 1-sigma and 2-sigma confidence intervals. Blue plots represent the case where spin is a variable parameter in the analysis and orange plots represent the case when spin is put to 0 in the template.

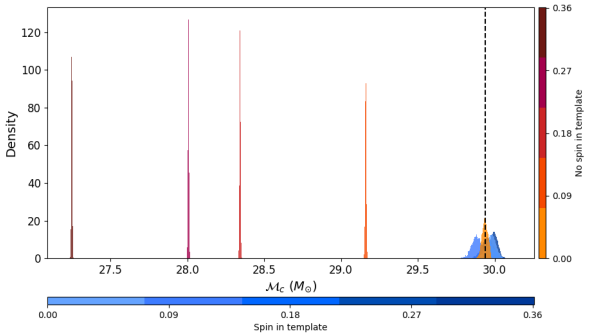

(a) Histograms for chirp mass for all spin cases plotted for spin considered in template (blue) and no spin considered in template (orange). The black dotted line represents the injected value of the chirp mass ($\mathcal{M}_c$).

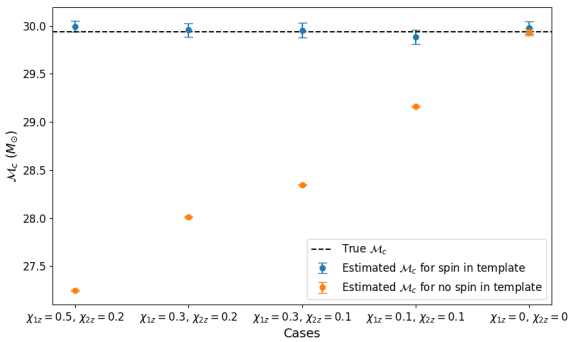

(b) Estimated chirp mass for all spin values for spin considered in template (blue) and no spin considered in template (orange). The black dotted line represents the injected value of the chirp mass ($\mathcal{M}_c$), while error bars indicate a 2σ interval.

Figure 3.6: Evolution of bias in estimation of chirp mass with different spin values.

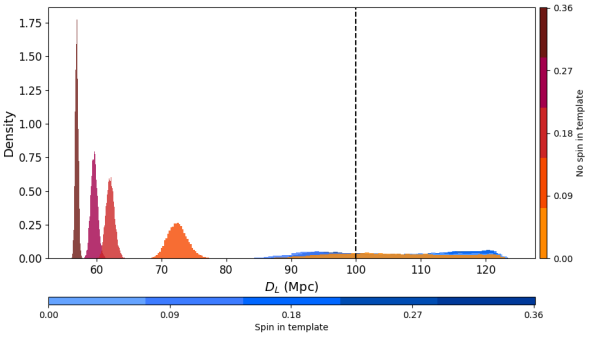

(a) Histograms for luminosity distance for all spin cases plotted for spin considered in template (blue) and no spin considered in template (orange). The black dotted line represents the injected value of the luminosity distance (D_L).

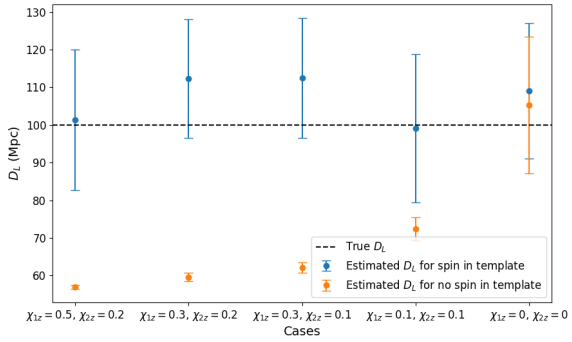

(b) Estimated luminosity distance for all spin values for spin considered in template (blue) and no spin considered in template (orange). The black dotted line represents the injected value of the luminosity distance (D_L), while error bars indicate a 2σ interval.

Figure 3.7: Evolution of bias in estimation of luminosity distance with different spin values.

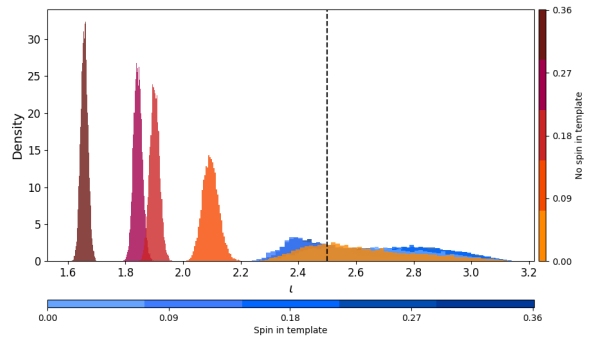

(a) Histograms for inclination for all spin cases plotted for spin considered in template (blue) and no spin considered in template (orange). The black dotted line represents the injected value of the inclination (ι).

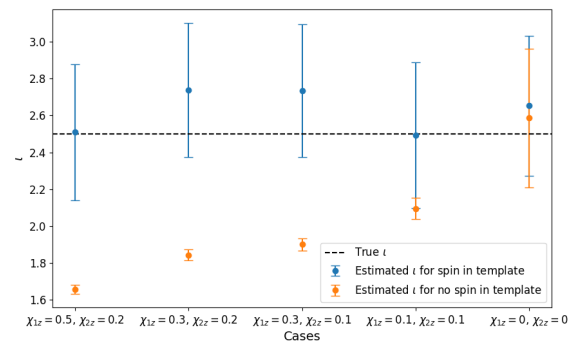

(b) Estimated inclination for all spin values for spin considered in template (blue) and no spin considered in template (orange). The black dotted line represents the injected value of the inclination (ι), while error bars indicate a 2σ interval.

Figure 3.8: Evolution of bias in estimation of inclination with different spin values.

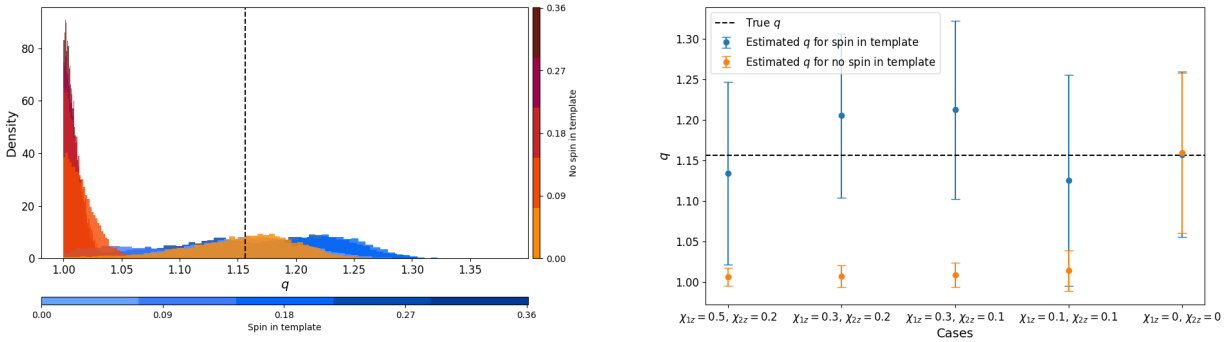

(a) Histograms for mass ratio for all spin cases plotted for spin considered in template (blue) and no spin considered in template (orange). The black dotted line represents the injected value of the mass ratio (q).

(b) Estimated mass ratio for all spin values for spin considered in template (blue) and no spin considered in template (orange). The black dotted line represents the injected value of the mass ratio (q), while error bars indicate a 2σ interval.

Figure 3.9: Evolution of bias in estimation of mass ratio with different spin values.

3.2 Eccentricity Mismodeling

Here, we present the results of our analysis to study the effect of eccentricity mismodeling on recovering injected parameters. Adding eccentricity to the signal increases the number of parameters, consequently increasing the computational time for parameter estimation. Because of the high computational time, we are unable to conduct tests for eccentricity mismodeling for a large number of cases and are forced to restrict to $e = 0, 0.1$, but we see an expected result here–mismodeling affects the estimation of spins and masses the most.

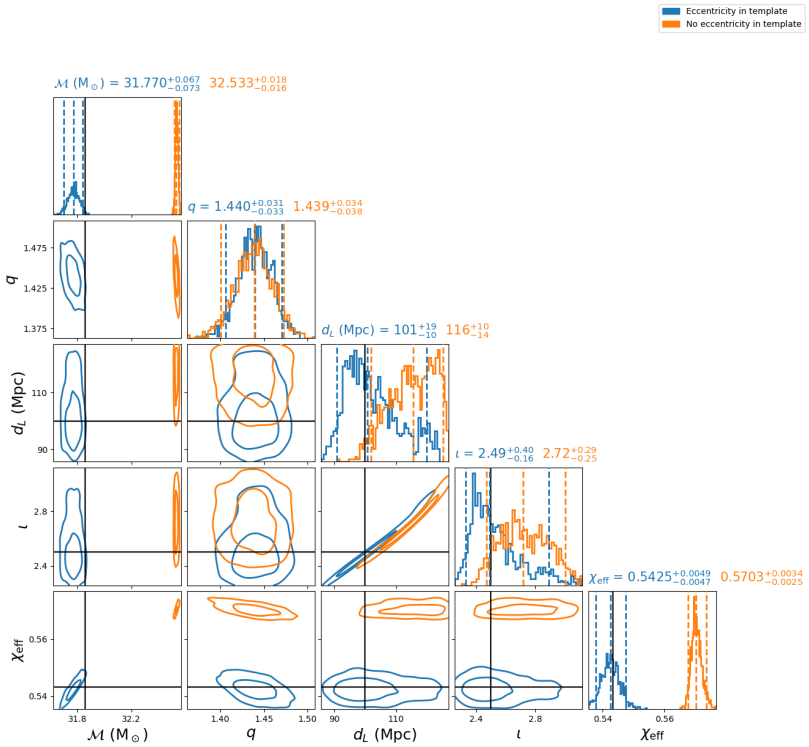

Figure 3.10: Parameter posterior corner plot of injected stellar-mass signal with eccentricity 0.1 in Gaussian stationary noise. Black lines represent the injected parameter values of the signal. The tiles at the top of each column display the median and 90% range for each inference. The contour in the 2D tiles represents the 1-sigma and 2-sigma confidence intervals. Blue plots represent the case where eccentricity is a variable parameter in the analysis and orange plots represent the case when eccentricity is put to 0 in the template.

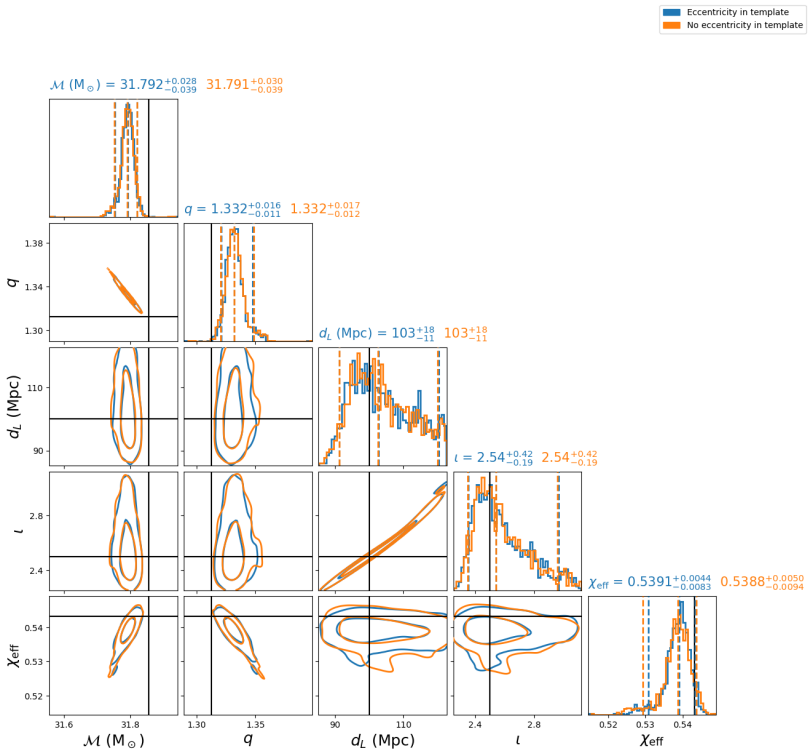

Figure 3.11: Parameter posterior corner plot of injected stellar-mass signal with eccentricity 0 in Gaussian stationary noise. Black lines represent the injected parameter values of the signal. The tiles at the top of each column display the median and 90% range for each inference. The contour in the 2D tiles represents the 1-sigma and 2-sigma confidence intervals. Blue plots represent the case where eccentricity is a variable parameter in the analysis and orange plots represent the case when eccentricity is put to 0 in the template.

4 Discussion

Our study, which investigates the impact of parameter mismodeling, holds significant importance in the advancement of new waveform development. It underscores the critical necessity for precise parameter modeling, thereby highlighting the essential role of accuracy in this aspect of research. It also highlights the need for the development of fast and accurate waveforms to analyse ever-increasing steam of data from upcoming detectors like ET and LISA.

4.1 Conclusion

We have shown that the mismodeling of spin and eccentricity can have an effect on both intrinsic and extrinsic parameter recovery. From our observations, we see that even the slightest discrepancy in waveform modeling can introduce bias into the estimated parameters. This bias persists even for small values of parameters (spin and eccentricity in our study), emphasizing the critical need for accurate modeling across all parameters and all parameter ranges. Although we explore an extreme case of mismodeling in this study, the presence of bias in estimated parameters resulting from mismodeled spin and eccentricity underscores the broader implication that any parameter mismodeling can induce bias. Notably, the induced bias in parameters becomes more pronounced for detectors with higher sensitivity, such as the ET, capable of detecting signals with higher signal-to-noise ratios (SNRs) compared to LIGO, which was the focus of our analysis. This study can evidently be treated as a proof of concept for more detailed studies to estimate the effect of parameter mismodeling for different binary systems and across various parameters. It motivates the need for accurate waveform modeling for parameter estimation for current and future detectors.

4.2 Limitations

Our analysis is restricted to a widely segmented range of spins and eccentricity and will become more conclusive with a greater number of tests. The drastic increase in the computation time with the addition of eccentricity prevented us from studying more cases.

4.3 Future Outlook

This study serves as a basis for further studies with higher-mass systems like MBHBs, which will be the primary target of LISA. We can expand on this analysis and produce concrete and conclusive results by using a much higher number of samples. Parameters like phase at coalescence, right ascension, and declination should also be varied for a full parameter estimation study.

Bibliography

[1] The LIGO Scientific Collaboration et al. "Advanced LIGO". In: *Classical and Quantum Gravity* 32.7 (Mar. 2015), p. 074001. DOI: 10.1088/0264-9381/32/7/074001. URL: https://dx.doi.org/10.1088/0264-9381/32/7/074001.

[2] B. P. Abbott et al. "GW170814: A Three-Detector Observation of Gravitational Waves from a Binary Black Hole Coalescence". In: *Physical Review Letters* 119.14 (Oct. 2017). ISSN: 1079-7114. DOI: 10.1103/physrevlett.119.141101. URL: http://dx.doi.org/10.1103/PhysRevLett.119.141101.

[3] T. Akutsu et al. *Overview of KAGRA: Calibration, detector characterization, physical environmental monitors, and the geophysics interferometer*. 2021. arXiv: 2009.09305 [gr-qc].

[4] Michele Maggiore et al. "Science case for the Einstein telescope". In: *Journal of Cosmology and Astroparticle Physics* 2020.03 (Mar. 2020), p. 050. DOI: 10.1088/1475-7516/2020/03/050. URL: https://dx.doi.org/10.1088/1475-7516/2020/03/050.

[5] Evan D. Hall. "Cosmic Explorer: A Next-Generation Ground-Based Gravitational-Wave Observatory". In: *Galaxies* 10.4 (2022). ISSN: 2075-4434. DOI: 10.3390/galaxies10040090. URL: https://www.mdpi.com/2075-4434/10/4/90.

[6] Pau Amaro-Seoane et al. *Laser Interferometer Space Antenna*. 2017. arXiv: 1702.00786 [astro-ph.IM].

[7] Jun Luo et al. "TianQin: a space-borne gravitational wave detector". In: *Classical and Quantum Gravity* 33.3 (Jan. 2016), p. 035010. DOI: 10.1088/0264-9381/33/3/035010. URL: https://dx.doi.org/10.1088/0264-9381/33/3/035010.

[8] S. Babak et al. "Searching for gravitational waves from binary coalescence". In: *Physical Review D* 87.2 (Jan. 2013). ISSN: 1550-2368. DOI: 10.1103/physrevd.87.024033. URL: http://dx.doi.org/10.1103/PhysRevD.87.024033.

[9] J. Veitch et al. "Parameter estimation for compact binaries with ground-based gravitational-wave observations using the LALInference software library". In: *Physical Review D* 91.4 (Feb. 2015). ISSN: 1550-2368. DOI: 10.1103/physrevd.91.042003. URL: http://dx.doi.org/10.1103/PhysRevD.91.042003.

[10] Nicolás Yunes and Xavier Siemens. "Gravitational-Wave Tests of General Relativity with Ground-Based Detectors and Pulsar-Timing Arrays". In: *Living Reviews in Relativity* 16.1 (Nov. 2013). ISSN: 1433-8351. DOI: 10.12942/lrr-2013-9. URL: http://dx.doi.org/10.12942/lrr-2013-9.

[11] Gianfranco Bertone et al. "Gravitational wave probes of dark matter: challenges and opportunities". In: *SciPost Physics Core* 3.2 (Oct. 2020). ISSN: 2666-9366. DOI: 10.21468/scipostphyscore.3.2.007. URL: http://dx.doi.org/10.21468/SciPostPhysCore.3.2.007.

[12] Luc Blanchet. *Post-Newtonian Theory for Gravitational Waves*. 2024. arXiv: 1310.1528 [gr-qc].

[13] Abdul H. Mroué et al. "Catalog of 174 Binary Black Hole Simulations for Gravitational Wave Astronomy". In: *Physical Review Letters* 111.24 (Dec. 2013). ISSN: 1079-7114. DOI: 10.1103/physrevlett.111.241104. URL: http://dx.doi.org/10.1103/PhysRevLett.111.241104.

[14] Karan Jani et al. "Georgia tech catalog of gravitational waveforms". In: *Classical and Quantum Gravity* 33.20 (Sept. 2016), p. 204001. ISSN: 1361-6382. DOI: 10.1088/0264-9381/33/20/204001. URL: http://dx.doi.org/10.1088/0264-9381/33/20/204001.

[15] Michael Boyle et al. "The SXS collaboration catalog of binary black hole simulations". In: *Classical and Quantum Gravity* 36.19 (Sept. 2019), p. 195006. ISSN: 1361-6382. DOI: 10.1088/1361-6382/ab34e2. URL: http://dx.doi.org/10.1088/1361-6382/ab34e2.

[16] Jonathan Blackman et al. "Fast and Accurate Prediction of Numerical Relativity Waveforms from Binary Black Hole Coalescences Using Surrogate Models". In: *Physical Review Letters* 115.12 (Sept. 2015). ISSN: 1079-7114. DOI: 10.1103/physrevlett.115.121102. URL: http://dx.doi.org/10.1103/PhysRevLett.115.121102.

[17] Vijay Varma et al. "Surrogate models for precessing binary black hole simulations with unequal masses". In: *Physical Review Research* 1.3 (Oct. 2019). ISSN: 2643-1564. DOI: 10.1103/physrevresearch.1.033015. URL: http://dx.doi.org/10.1103/PhysRevResearch.1.033015.

[18] Michael Pürrer. "Frequency-domain reduced order models for gravitational waves from aligned-spin compact binaries". In: *Classical and Quantum Gravity* 31.19 (Sept. 2014), p. 195010. ISSN: 1361-6382. DOI: 10.1088/0264-9381/31/19/195010. URL: http://dx.doi.org/10.1088/0264-9381/31/19/195010.

[19] D. Williams et al. "Precessing numerical relativity waveform surrogate model for binary black holes: A Gaussian process regression approach". In: *Physical Review D* 101.6 (Mar. 2020). ISSN: 2470-0029. DOI: 10.1103/physrevd.101.063011. URL: http://dx.doi.org/10.1103/PhysRevD.101.063011.

[20] Scott E. Field et al. "Fast Prediction and Evaluation of Gravitational Waveforms Using Surrogate Models". In: *Physical Review X* 4.3 (July 2014). ISSN: 2160-3308. DOI: 10.1103/physrevx.4.031006. URL: http://dx.doi.org/10.1103/PhysRevX.4.031006.

[21] A. Buonanno and T. Damour. "Effective one-body approach to general relativistic two-body dynamics". In: *Physical Review D* 59.8 (Mar. 1999). ISSN: 1089-4918. DOI: 10.1103/physrevd.59.084006. URL: http://dx.doi.org/10.1103/PhysRevD.59.084006.

[22] Patricia Schmidt. "Gravitational Waves From Binary Black Hole Mergers: Modeling and Observations". In: *Frontiers in Astronomy and Space Sciences* 7 (2020). ISSN: 2296-987X. DOI: 10.3389/fspas.2020.00028. URL: https://www.frontiersin.org/articles/10.3389/fspas.2020.00028.

[23] Alessandra Buonanno. *The end of the cosmic dawn*. June 2022. URL: https://www.mpg.de/18720037/the-end-of-the-cosmic-dawn.

[24] Lionel London et al. "First Higher-Multipole Model of Gravitational Waves from Spinning and Coalescing Black-Hole Binaries". In: *Physical Review Letters* 120.16 (Apr. 2018). ISSN: 1079-7114. DOI: 10.1103/physrevlett.120.161102. URL: http://dx.doi.org/10.1103/PhysRevLett.120.161102.

[25] Salvatore Vitale and Hsin-Yu Chen. "Measuring the Hubble Constant with Neutron Star Black Hole Mergers". In: *Physical Review Letters* 121.2 (July 2018). ISSN: 1079-7114. DOI: 10.1103/physrevlett.121.021303. URL: http://dx.doi.org/10.1103/PhysRevLett.121.021303.

[26] Will M. Farr et al. "Distinguishing spin-aligned and isotropic black hole populations with gravitational waves". In: *Nature* 548.7668 (Aug. 2017), pp. 426–429. ISSN: 1476-4687. DOI: 10.1038/nature23453. URL: http://dx.doi.org/10.1038/nature23453.

[27] Ben Farr, Daniel E. Holz, and Will M. Farr. "Using Spin to Understand the Formation of LIGO and Virgo's Black Holes". In: *The Astrophysical Journal Letters* 854.1 (Feb. 2018), p. L9. ISSN: 2041-8213. DOI: 10.3847/2041-8213/aaaa64. URL: http://dx.doi.org/10.3847/2041-8213/aaaa64.

[28] Sylvia Biscoveanu, Colm Talbot, and Salvatore Vitale. "The effect of spin mismodelling on gravitational-wave measurements of the binary neutron star mass distribution". In: *Monthly Notices of the Royal Astronomical Society* 511.3 (Feb. 2022), pp. 4350–4359. ISSN: 0035-8711. DOI: 10.1093/mnras/stac347. eprint: https://academic.oup.com/mnras/article-pdf/511/3/4350/42600955/stac347.pdf. URL: https://doi.org/10.1093/mnras/stac347.

[29] Ken K. Y. Ng et al. "Gravitational-wave astrophysics with effective-spin measurements: Asymmetries and selection biases". In: *Phys. Rev. D* 98 (8 Oct. 2018), p. 083007. DOI: 10.1103/PhysRevD.98.083007. URL: https://link.aps.org/doi/10.1103/PhysRevD.98.083007.

[30] Curt Cutler and Éanna E. Flanagan. "Gravitational waves from merging compact binaries: How accurately can one extract the binary's parameters from the inspiral waveform?" In: *Physical Review D* 49.6 (Mar. 1994), pp. 2658–2697. ISSN: 0556-2821. DOI: 10.1103/physrevd.49.2658. URL: http://dx.doi.org/10.1103/PhysRevD.49.2658.

[31] Michael Zevin et al. "Eccentric Black Hole Mergers in Dense Star Clusters: The Role of Binary–Binary Encounters". In: *The Astrophysical Journal* 871.1 (Jan. 2019), p. 91. ISSN: 1538-4357. DOI: 10.3847/1538-4357/aaf6ec. URL: http://dx.doi.org/10.3847/1538-4357/aaf6ec.

[32] Carl L. Rodriguez et al. "Black holes: The next generation—repeated mergers in dense star clusters and their gravitational-wave properties". In: *Physical Review D* 100.4 (Aug. 2019). ISSN: 2470-0029. DOI: 10.1103/physrevd.100.043027. URL: http://dx.doi.org/10.1103/PhysRevD.100.043027.

[33] Carl L. Rodriguez, Sourav Chatterjee, and Frederic A. Rasio. "Binary black hole mergers from globular clusters: Masses, merger rates, and the impact of stellar evolution". In: *Phys. Rev. D* 93 (8 Apr. 2016), p. 084029. DOI: 10.1103/PhysRevD.93.084029. URL: https://link.aps.org/doi/10.1103/PhysRevD.93.084029.

[34] Daniel J D'Orazio and Johan Samsing. "Black hole mergers from globular clusters observable by LISA II. Resolved eccentric sources and the gravitational wave background". In: *Monthly Notices of the Royal Astronomical Society* 481.4 (Sept. 2018), pp. 4775–4785. ISSN: 0035-8711. DOI: 10.1093/mnras/sty2568. eprint: https://academic.oup.com/mnras/article-pdf/481/4/4775/25981896/sty2568.pdf. URL: https://doi.org/10.1093/mnras/sty2568.

[35] Marc Favata. "Systematic Parameter Errors in Inspiraling Neutron Star Binaries". In: *Physical Review Letters* 112.10 (Mar. 2014). ISSN: 1079-7114. DOI: 10.1103/physrevlett.112.101101. URL: http://dx.doi.org/10.1103/PhysRevLett.112.101101.

[36] Nelson Christensen and Renate Meyer. "Parameter estimation with gravitational waves". In: *Reviews of Modern Physics* 94.2 (Apr. 2022). ISSN: 1539-0756. DOI: 10.1103/revmodphys.94.025001. URL: http://dx.doi.org/10.1103/RevModPhys.94.025001.

[37] Percy artist Moran and Peter Whittle. "Hypothesis Testing in Time Series Analysis." In: 1951. URL: https://api.semanticscholar.org/CorpusID:125739077.

[38] Nicholas Metropolis and S. Ulam. "The Monte Carlo method". In: 44.247 (Sept. 1949), pp. 335–341. ISSN: 0162-1459 (print), 1537-274X (electronic). DOI: https://doi.org/10.2307/2280232. URL: http://links.jstor.org/sici?sici=0162-1459%28194909%2944%3A247%3C335%3ATMCM%3E2.0.CO%3B2-3;%20http://www.jstor.org/stable/2280232.

[39] John Skilling. "Nested sampling for general Bayesian computation". In: *Bayesian Analysis* 1.4 (2006), pp. 833–859. DOI: 10.1214/06-BA127. URL: https://doi.org/10.1214/06-BA127.

[40] Nicholas Metropolis et al. "Equation of State Calculations by Fast Computing Machines". In: *The Journal of Chemical Physics* 21.6 (June 1953), pp. 1087–1092. ISSN: 0021-9606. DOI: 10.1063/1.1699114. eprint: https://pubs.aip.org/aip/jcp/article-pdf/21/6/1087/18802390/1087_1_online.pdf. URL: https://doi.org/10.1063/1.1699114.

[41] URL: https://coma.kasi.re.kr/nrgwss2021/resource/lecture_data/data_analysis_v5_2021NR_School.pdf.

[42] C. M. Biwer et al. "PyCBC Inference: A Python-based parameter estimation toolkit for compact binary coalescence signals". In: *Publ. Astron. Soc. Pac.* 131.996 (2019), p. 024503. DOI: 10.1088/1538-3873/aaef0b. arXiv: 1807.10312 [astro-ph.IM].

[43] Sebastian Khan et al. "Frequency-domain gravitational waves from nonprecessing black-hole binaries. II. A phenomenological model for the advanced detector era". In: *Physical Review D* 93.4 (Feb. 2016). ISSN: 2470-0029. DOI: 10.1103/physrevd.93.044007. URL: http://dx.doi.org/10.1103/PhysRevD.93.044007.

[44] Akshita Mittal. *teobecc: PyCBC plugin for parameter estimation of eccentric, spinning signals*. https://github.com/drnkyda/teobecc. [Accessed 05-04-2024].

[45] Daniel Foreman-Mackey et al. "¡tt¿emcee¡/tt¿: The MCMC Hammer". In: *Publications of the Astronomical Society of the Pacific* 125.925 (Mar. 2013), pp. 306–312. ISSN: 1538-3873. DOI: 10.1086/670067. URL: http://dx.doi.org/10.1086/670067.

[46] W. D. Vousden, W. M. Farr, and I. Mandel. "Dynamic temperature selection for parallel tempering in Markov chain Monte Carlo simulations". In: *Monthly Notices of the Royal Astronomical Society* 455.2 (Nov. 2015), pp. 1919–1937. ISSN: 0035-8711. DOI: 10.1093/mnras/stv2422. eprint: https://academic.oup.com/mnras/article-pdf/455/2/1919/18514064/stv2422.pdf. URL: https://doi.org/10.1093/mnras/stv2422.

[47] Joshua S Speagle. "dynesty: a dynamic nested sampling package for estimating Bayesian posteriors and evidences". In: *Monthly Notices of the Royal Astronomical Society* 493.3 (Feb. 2020), pp. 3132–3158. ISSN: 1365-2966. DOI: 10.1093/mnras/staa278. URL: http://dx.doi.org/10.1093/mnras/staa278.

[48] Danilo Chiaramello and Alessandro Nagar. "Faithful analytical effective-one-body waveform model for spin-aligned, moderately eccentric, coalescing black hole binaries". In: *Phys. Rev. D* 101 (10 May 2020), p. 101501. DOI: 10.1103/PhysRevD.101.101501. URL: https://link.aps.org/doi/10.1103/PhysRevD.101.101501.

[49] *PyCBC inference documentation (pycbc.inference) &x2014; PyCBC 2.4.dev1 documentation — pycbc.org*. https://pycbc.org/pycbc/latest/html/inference.html. [Accessed 29-03-2024].